

Two-stage electron acceleration by 3D collisionless guide field magnetic reconnection

P. A. Muñoz^{a)} and J. Büchner

Max-Planck-Institut für Sonnensystemforschung, D-37077 Göttingen, Germany^{b)}

(Dated: December 14, 2024)

The mechanism of electron acceleration to high energies is crucial, e.g., for space and astrophysics. Magnetic reconnection was suggested but its efficiency as an electron accelerator is not proven yet, especially for non-relativistic electron-proton plasmas. We now have found that 3D turbulent guide-field magnetic reconnection accelerates electrons to high energies in a two-stage non-linear process. After the electrons are first pre-accelerated, as well-known, by the magnetic field aligned (parallel) reconnection electric field, they become additionally accelerated by a Fermi-type process in magnetic-field-aligned filamentary structures which form out of the kinetic turbulence which is self-generated by reconnection. A power-law spectrum of energetic electrons forms with a spectral index of the order of -1.5. Therefore, even single-X-line, non-relativistic collisionless 3D guide field reconnection can efficiently further energize electrons due to Fermi-acceleration in 3D filamentary structures.

Introduction.— In the Universe electrons are ubiquitously accelerated to high energies. They are diagnosed by the high-frequency electromagnetic radiation of a wide variety of astrophysical objects but also directly detected by in-situ spacecrafts observations. Energetic electrons cause, e.g., radio waves and hard X-ray emissions from the chromospheric footpoints of magnetic arcs during solar flares^{1,2}. In-situ spacecraft observations provide directly the spectra of energetic electrons, as well as information about the local plasma and magnetic fields which are usually highly turbulent at the acceleration sites (see, e.g.,³). The current MMS mission⁴, e.g., directly associated electron acceleration with a broadband turbulence⁵⁻⁷. Common for those observations is the presence of current sheets (CSs) and magnetic reconnection through them, possibly accelerating electrons at the expense of the annihilation of magnetic flux and magnetic energy^{8,9}.

In the past a number of theoretical conjectures was made about the mechanisms of electron acceleration by reconnection, and test particle calculations were carried out to verify the suggested electron acceleration mechanisms. Test particle calculations usually use prescribed electromagnetic fields or those obtained by MHD simulations. In them, electrons are energized, mainly by the magnetic-field-aligned reconnection electric fields near single¹⁰⁻¹² or multiple X-lines^{13,14}, in stochastic current sheets^{15,16} or in turbulence^{17,18}. Test particle calculations usually overestimate, however, the electron acceleration, assuming reconnection electric fields which are not calculated self-consistently. Instead, ad-hoc assumptions about a finite (“anomalous”) resistivity are made. For already relativistic (electron-proton) plasmas, self-consistent fully-kinetic PiC-code simulations considered electron acceleration in 2D-¹⁹⁻²¹ and 3D-²² magnetic re-

connection. It is, however, not clear, yet, how reconnection can efficiently accelerate thermal electrons of space and astrophysical plasmas up to relativistic energies. Non-relativistic 2D PiC-code simulations revealed, e.g., only weak electron acceleration due to the reconnection electric field. Electrons might additionally be accelerated by surfing or due to parallel electric fields in the separatrices or outflow region of reconnection²³⁻²⁶. 2D PiC-code simulations of long current sheets provided evidence of first order Fermi-type acceleration in contracting magnetic islands (plasmoids), or stochastic Fermi acceleration due to the interaction of multiple magnetic islands in turbulent reconnecting plasmas²⁷⁻³³. This idea was supported by theoretical models³⁴ and evidenced by solar wind observations³⁵. In 3D plasmoid reconnection, electrons can be energized more efficiently if the particles are not confined in closed contracting magnetic islands as in 2D³⁶. This kind of Fermi acceleration is, however, suppressed in strongly magnetized (low plasma- β) astrophysical plasmas, such as those of solar coronal current sheets dominated by strong magnetic guide-fields. In addition, all previous investigations did not take into account the self-consistently generated 3D turbulence and consequent nonlinear structures formation in the current direction. Does the self-generated turbulence reduce the electron energy by wave-particle interactions or can it even enhance their energization? What are the consequences of non-linear structure formation processes?

Simulation.— We addressed the question of electron acceleration due to its interaction with the self-generated turbulence and structures in 3D guide-field magnetic reconnection through force-free current sheets³⁷. We demonstrate our findings by utilizing the fully-kinetic relativistic PiC-code ACRONYM³⁸. The use of two current sheets allows periodic boundary conditions in all the three directions. We illustrate our findings by showing results of a simulation run (carried out among a number of similar ones) with the following parameters: an ion-electron mass ratio $m_i/m_e = 100$, equal electron and ion temperatures $T_i/T_e = 1.0$ except for

^{a)}Electronic mail: munozp@mps.mpg.de

^{b)}Max-Planck/Princeton Center for Plasma Physics

Fig. 4b), which was obtained for $T_i/T_e = 5.0$ to discuss the temperature dependence, a plasma beta $\beta_e = \beta_i = 2\mu_0 n_0 k_B T_i / B_T^2 = 0.08$ and a relative guide field strength $b_g = B_g / B_{\infty y} = 2$. Here, $B_{\infty y}$ is the asymptotic magnetic field and $B_T = B_{\infty y} \sqrt{1 + b_g^2}$ is the (initially constant) total magnetic field. The current sheet halfwidth is $L = 0.25d_i$ (where $d_i = c/\omega_{pi}$ is the ion inertial length and ω_{pi} is the ion plasma frequency). The initial ion and electron number densities are constant and equal ($n_i = n_e = n_0$). The plasma is represented by 50 macroparticles per cell (ppc), 25 per specie. This number is necessary, since for a smaller number of ppc, numerical thermalization would obscure the particle acceleration³⁹. In the example further discussed here, the simulation box $L_x \times L_y \times L_z$ covers a physical domain $4d_i \times 8d_i \times 16d_i$. The numerical mesh spans $256 \times 512 \times 1024$ grid points. We triggered reconnection by an initial magnetic field perturbation, narrowly localized in the current direction (z), and with a long-wavelength tearing mode in the y -direction. Since we wanted to illustrate the efficiency of the non-linear acceleration of electrons even at a single reconnection site, we intentionally choose a sufficiently short box in the CS y -direction, such that multiple X-lines and flux ropes cannot be formed.

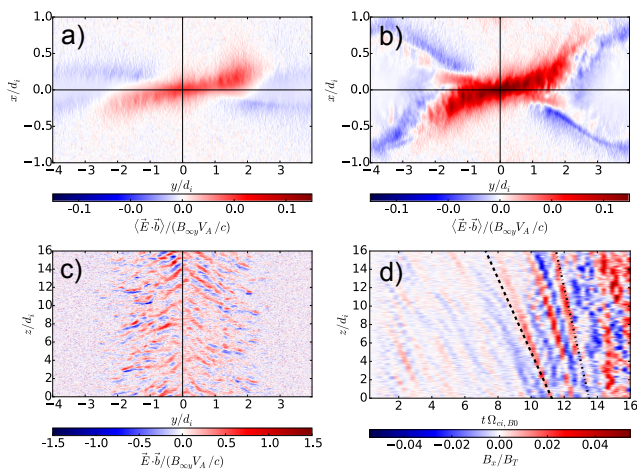


Figure 1. a) and b) Spatial distribution of $\langle E_{\parallel} \rangle$, the parallel electric field $E_{\parallel}(x, y)$ averaged over z , a) at $t = 10 \Omega_{ci}^{-1}$ and b) at $t = 13.5 \Omega_{ci}^{-1}$. c) Spatial distribution of $E_{\parallel}(y, z)$ in the CS central plane ($x = 0$) at $t = 13.5 \Omega_{ci}^{-1}$. d) Temporal evolution of the perpendicular magnetic fluctuations B_x along $x = y = 0$. The slope of the dashed line indicates the initial electron drift speed, that of the dashed-dotted line to twice the electron drift speed.

Results.— It is well known that electrons are accelerated by the parallel reconnection electric field E_{\parallel} in the guide field direction. Figs. 1a)-b) show the spatial distribution of $\langle E_{\parallel} \rangle$, the averaged over the z direction reconnection electric field, in the plane $x - y$, at two characteristic times. Note that these and the following contour plots show time-averaged over $0.1 \Omega_{ci}$ quanti-

ties, in order to diminish the high-frequency PiC shot noise. In the plane $x - y$, $\langle E_{\parallel} \rangle$ has a typical guide-field reconnection structure. The maximum $\langle E_{\parallel} \rangle$ and the reconnection rate are similar. They vary between $\langle E_{\parallel} \rangle = 0.08E_0$ at $t = 10 \Omega_{ci}^{-1}$ and $0.15E_0$ at $t = 13.5 \Omega_{ci}^{-1}$ (where $E_0 = V_A B_{\infty y}$ and V_A is the Alfvén speed on $B_{\infty y}$). During the first stage of the evolution of 3D guide-field reconnection, the parallel electric field $\langle E_{\parallel} \rangle$ mildly pre-accelerates electrons. The growing current-streaming and shear-flow-driven self-generated turbulence, leads at its non-linear stage to a filamentation of E_{\parallel} and of the reconnection magnetic field B_x along the guide-field direction (z). Fig. 1c) shows the spatially structured $E_{\parallel}(y, z)$ with alternating directions (signs as red/blue colors) in the central plane $x = 0$ (the CS center) at $t = 13.5 \Omega_{ci}^{-1}$. At this stage, the maximum value of the parallel electric field is $|E_{\parallel, max}| = 1.5E_0$, exceeding the average parallel electric field $\langle E_{\parallel} \rangle$, obtained by taking into account the alternating signs of E_{\parallel} , by a factor of ten. The work of the electromagnetic field on the particles ($\vec{j} \cdot \vec{E}$) and the associated dissipation are filamentary structured in the same way as E_{\parallel} (diagnostics not shown here). Note that similar structures were previously found by PiC-code simulations of 3D magnetic reconnection, both near X-lines^{40–43} and near separatrices^{44–46}. Observations in the Earth’s magnetosphere confirmed them^{47–49}. The process of structure formation out of turbulence is illustrated by Fig. 1d) for the magnetic field $B_x(z)$ along the X-line $x = y = 0$. Fig. 1d) shows the evolution of the filamentary structures in the magnetic field, which is more clear (smoother) than the parallel electric field E_{\parallel} , noisy as typical for PiC codes. The slopes of the dashed and dotted lines correspond to the initial (current-carrying) electron drift speed ($V_{De} \sim 4V_A$) and twice that value, respectively. As one can see in Fig. 1d), after $t = 13.5 \Omega_{ci}^{-1}$ the electron drift speed increases in the course of the non-linear evolution of reconnection, i.e., while the CS thins down the propagation of the filamentary structures accelerates, as the characteristic speed of the propagating turbulence increases. The characteristic propagation speed of the filamentary structures is proportional to the electron drift forming the CS. It reminds the spreading of reconnection previously obtained by two-fluid investigations⁵⁰, in experiments⁵¹, in 3D numerical Hall-code simulations⁵², EMHD⁵³ and fully-kinetic 3D simulations of Harris-type current sheets^{54,55}. According to them, reconnection spreads with the fastest velocity of either the electron drift speed ($4V_A$ in our case) which equals the diamagnetic drift speed in Harris current sheets, or the Alfvén speed based on the guide field ($2V_A$). While the structures in the weak guide field case are driven by the electron motion, they are controlled by propagating Alfvén waves in the case of strong guide-fields $b_g \gtrsim d_i/L$ ($= 4$ for our parameters).

In the traveling filamentary structures, electrons are first of all accelerated and decelerated in dependence on the signs of the local parallel electric field E_{\parallel} . Due to the finite guide magnetic field, the contributions to the gain

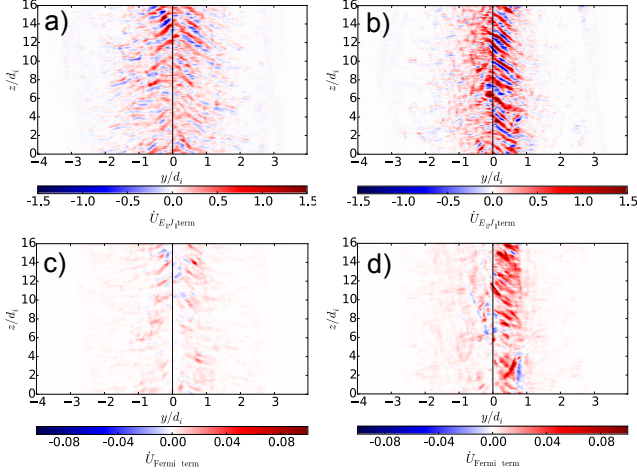


Figure 2. Rate of energy change of electrons crossing the CS central plane ($x = 0$). Shown are the contributions of the first two terms of Eq. 1. Upper row: $E_{\parallel}J_{\parallel}$ due to parallel electric fields at a) $t = 13.5\Omega_{ci}^{-1}$ and b) $t = 15\Omega_{ci}^{-1}$. Lower row: Energy change of the Fermi-type acceleration at a) $t = 13.5\Omega_{ci}^{-1}$. and d) $t = 15\Omega_{ci}^{-1}$.

and loss of the electron energy can be quantified in the framework of the guiding-center approximation^{31,56}:

$$\frac{dU}{dt} = E_{\parallel}J_{\parallel} + \left(p_{e,\parallel} + m_e n_e u_{e,\parallel}^2 \right) \vec{u}_{\vec{E}} \cdot \vec{\kappa} \quad (1)$$

$$+ \frac{p_{e,\perp}}{B} \left(\frac{\partial B}{\partial t} + \vec{u}_{\vec{E}} \cdot \vec{\nabla} B \right).$$

Here U is the electron kinetic energy density, $\vec{u}_{\vec{E}}$ is the $\vec{E} \times \vec{B}$ drift speed, $p_{e,\parallel}$ ($p_{e,\perp}$) are the parallel (and perpendicular, respectively) electron pressure, $u_{e,\parallel}$ is the parallel electron bulk flow velocity and $\vec{\kappa} = (\vec{B}/B) \cdot \vec{\nabla}(\vec{B}/B)$ is the curvature of the magnetic field. The first term on the right-hand side (r.h.s) of Eq. (1) describes the effect of parallel electric fields, the second is curvature-related, allowing bouncing and therefore Fermi-type acceleration, and the third is due to magnetic field inhomogeneities via conservation of the adiabatic invariant magnetic moment. Figs. 2 shows the spatial distribution of the first two contributions to the acceleration (top and bottom rows) obtained in the CS central plane $x = 0$ at two different times ($t = 13.5\Omega_{ci}^{-1}$ and $t = 15\Omega_{ci}^{-1}$, left and right columns, respectively). The third term in the r.h.s. of Eq. (1), related to the magnetic field inhomogeneities, is not shown since it is negligible: it is everywhere an order of magnitude smaller than the smallest of the first two terms in the r.h.s of Eq. (1). In Figs. 2, the change of the electron energy density dU/dt is normalized to $E_0 J_0$ (where $J_0 = en_e v_{th,e}$). As one can see, comparing panels a)-b) and c)-d) in Fig. 2, the parallel electric field term locally changes the electron energy much stronger than the Fermi-type process. But on average, the Fermi-type acceleration due to the curvature of the filaments' magnetic field, however, accelerates the

electrons much more efficiently than the parallel reconnection electric fields. Let us compare the net effects of electron energy change by calculating an effective acceleration electric field. The one which corresponds to the Fermi-type process is $E_{\text{eff}} \sim 0.1E_0$ at $t = 13.5\Omega_{ci}^{-1}$, in the beginning comparable with the average parallel electric field and the reconnection rate. The effective acceleration electric field E_{eff} increases, however, by another factor of two until $t = 15\Omega_{ci}^{-1}$, despite of the energy gain by parallel electric fields not changing significantly any more. While the Fermi-type process permanently causes a positive net-acceleration of the electrons, the parallel electric fields subsequently accelerate and decelerate the particles (c.f. the opposite signs shown by blue/red colors in Fig. 1c)), with a small net acceleration effect. Note that near the low-density separatrix, the Fermi-type acceleration dominates even more, while the contribution of the parallel electric field acceleration even decreases.

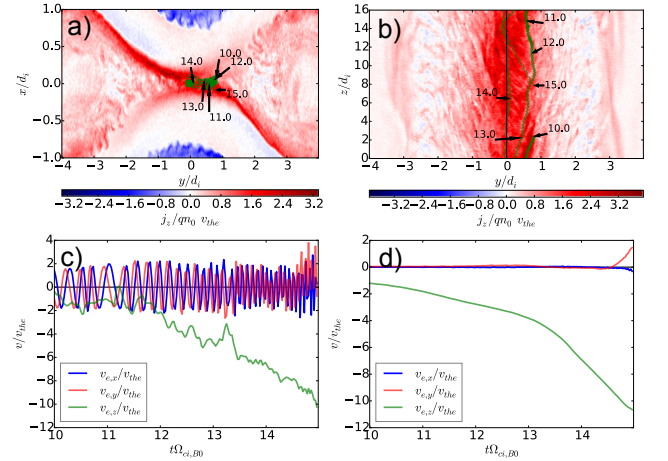


Figure 3. a) Projections of a typical energetic electron trajectories (green lines) to the $x-y$ plane (at $z = L_z/2$) and to the b) CS central plane $x = 0$. Subsequent electron positions are indicated by time marks (in units of Ω_{ci}^{-1}). The background colors depicts the current density j_z at $t_f = 15\Omega_{ci}^{-1}$. c) Evolution of the (four-)velocity components of the typical energetic electron (same as in a) and b)). d) Time history of the ensemble-averaged (four-)velocity components of the 10^4 most energetic electrons.

The panels a)-b) of Fig. 3 illustrate the transition to the nonlinear electron acceleration by showing the trajectory of a typical energized electron between $t_i = 10\Omega_{ci}^{-1}$ and $t_f = 15\Omega_{ci}^{-1}$ (green lines). One can see how the electron coming from the low-density separatrix enters the X-line region at t_i , remaining there for a while to become accelerated (in the $-z$ direction) by the parallel reconnection electric field. The two-stage acceleration can clearly be seen in the temporal evolution of the $v_{e,z}$ four-velocity component of this electron, for which the first acceleration stage lasts until $t \sim 12\Omega_{ci}^{-1}$ (c.f. Fig. 3c)). While being accelerated in the parallel electric field direction ($-z$), the charged particle continues

to gyrate (see the $v_{e,x}$ and $v_{e,y}$ components). For this particular electron, the second acceleration stage due to the Fermi process in the growing filaments starts at about $t \sim 12 \Omega_{ci}^{-1}$. For different electrons the Fermi-acceleration starts to dominate earlier or later, depending upon their phase space coordinates at the moment they enter the filaments. Fig. 3d) shows the evolution of the ensemble average velocity of the most energetic electrons. It confirms that, on average, the energy is gained by those electrons in a two-stage process. The most efficient acceleration takes place after $t \sim (12 - 13.4) \Omega_{ci}^{-1}$, i.e., when the filamentary structures are fully developed and the Fermi-type process completely dominates. Note that Fig. 3d) was generated by tracing back in time a total of 10^4 most energetic electrons located in a small domain near the X-line at $t \sim 15.0 \Omega_{ci}^{-1}$. Note also that the maximum electron velocity reached at $t = 15 \Omega_{ci}^{-1}$ is already relativistic: the four-velocity component $v_{e,z,max}$ implies a particle speed in the ordinary velocity space of $0.74c$, which corresponds to a relativistic Lorentz factor of $\gamma \sim 1.49$. The efficiency of the average acceleration of energetic electrons can be estimated by a linear fit of the increasing velocity $v_{e,z}$. Since the acceleration is proportional to the effective electric field multiplied by a factor e/m_e , one can relate it to an effectively accelerating electric field. During the pre-acceleration (up to $t \sim 12 \Omega_{ci}^{-1}$) predominantly in the E_{\parallel} field, it is just $E_{\text{eff}} \sim E_0$, while during the second, dominantly Fermi-type acceleration phase (until $t \sim 15.0 \Omega_{ci}^{-1}$), E_{eff} becomes as large as $6.0E_0$. The effective acceleration electric fields obtained for the ensemble of the 10^4 most energetic electrons are also similar to those found for the single electron trajectory (see Fig. 3d)): $E_{\text{eff}} \sim 2.0E_0$ before the clear change in the slope at $t \sim 13.4 \Omega_{ci}^{-1}$ and $E_{\text{eff}} \sim 8.2E_0$ after that. Hence, the effective electric fields which characterize the efficiency of the acceleration exceeds several times the maximum value of the parallel electric field near the X-line. Fig. 3c) also demonstrates how during the second acceleration phase, the electron gyrofrequency increases due to the interaction with the self-generated high-frequency (electron-scale) kinetic turbulence.

The resulting electron energy spectra obtained at $t = t_f$, when reconnection is fully developed, are shown in Fig. 4. For $T_i/T_e = 1$ at $t_f = 15 \Omega_{ci}^{-1}$ in Fig. 4a) and for an enhanced $T_i/T_e = 5$ at $t_f = 15 \Omega_{ci}^{-1}$ in Fig. 4b). The electrons are first of all heated: the blue dashed lines corresponds to a Maxwellian fit of the thermal part of the spectrum. The final electron thermal velocity exceeds the initial one by almost (20 – 40)% (depicted by brown dashed lines). The non-thermal tail of the electron distribution is best fitted by a power-law dependence $f(K) = K^{-\alpha}$ (red dashed line), where K is the electron kinetic energy. For an initial temperature ratio $T_i/T_e = 1$ (Fig. 4a)), the resulting spectral index is $\alpha = 1.55$, as often found by in-situ observations as well as for electrons detected via the hard X-ray emission of solar flares^{57,58}. The most energetic electrons within the power-law portion reach an order of magnitude above

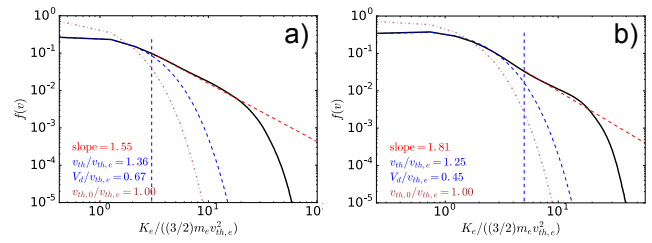


Figure 4. a) Spectra of energetic electrons accelerated by 3D reconnection at $t = t_f$, the time when reconnection is fully developed. a) for $T_i/T_e = 1$ at $t_f = 15 \Omega_{ci}^{-1}$. b) for $T_i/T_e = 5$ at $t_f = 10 \Omega_{ci}^{-1}$. The dashed-dotted lines correspond to the initial thermal distribution, the blue dashed lines are Maxwellian fits of the distribution at $t = t_f$ and the red dashed lines are power law fits of the energetic tail of the electrons distribution at $t = t_f$.

the initial thermal energy. The power-law portion of the spectrum ends with an exponential cutoff⁵⁹. The highest energies are reached by electrons approaching the center of reconnection. In the reconnection separatrixes and exhaust regions, fast electrons are thermalized via pitch-angle scattering in the self-generated lower-hybrid turbulence. Their spectra become dominated by a thermal distribution with high electron temperatures, without significant power-law portion.

Since the wavelength of the lower-hybrid waves and turbulence, from where the filamented structures grow, increases with the ions to electrons temperature ratio T_i/T_e , the characteristic length-scale of the Fermi-type acceleration and the magnetic field curvature should change with T_i/T_e as well: the Fermi-type acceleration should be less efficient the larger T_i/T_e is. The contribution of the parallel electric field acceleration, on the other hand, does not depend on T_i/T_e . We confirmed this theoretical prediction by repeating the simulation but with a higher temperature ratio of $T_i/T_e = 5$. As shown in Fig. 4b), the electron energy spectrum now is steeper, with a spectral index $\alpha \sim -1.8$.

Conclusions.— We have shown that collisionless turbulent 3D non-relativistic guide field magnetic reconnection energizes electrons very efficiently, at every X-line, due to a two-stage process consisting of a pre-acceleration in laminar parallel electric-fields followed by a non-linear stage dominated by Fermi-type acceleration after filamentary structures are formed out of the self-generated turbulence.

The resulting electron energy spectra are characterized by an enhanced electron temperature and a non-thermal high-energy tail. A power-law distribution is formed with a spectral index α depending on the temperature ratio T_i/T_e , $\alpha \sim -1.5$ for $T_i/T_e = 1$ and $\alpha \sim -1.8$ for $T_i/T_e = 5$. The laminar parallel reconnection electric field only pre-accelerates the electrons. Out of the self-generated turbulence, however, well expressed filamentary structures grow in the current (guide-field) direction, which increasingly cause a first-order Fermi acceleration

of the electrons beyond the energies which are caused by parallel reconnection electric fields. Since the Fermi-type acceleration is proportional to the electron speed, it becomes more efficient after the electrons are already pre-accelerated in the parallel electric fields. The main acceleration by 3D reconnection is, therefore, enhanced by the filamentary structures non-linearly formed out of the kinetic turbulence, which is due to self-generated current-aligned streaming instabilities. The acceleration is more efficient the more extended the reconnection region is in the current direction and the thinner the current sheets are, which provide the free energy for streaming instabilities causing the turbulence. Note that the Fermi-type acceleration described here does not rely on contracting islands or a plasmoid instability of long current sheets.

In order to compare our results for electron acceleration with test particle calculations based on resistive MHD simulations, we estimate an effective ("anomalous") resistivity η_{eff} as $\langle E_{\parallel} \rangle / \langle j_z \rangle$. It is $\eta_{\text{eff}} \sim 0.025 B_{\infty y} / (en_e)$ (with the Hall resistivity $B_{\infty y} / (en_e)$) near the X-line at $t = 13.5 \Omega_{ci}^{-1}$. This corresponds to an effective collision frequency $\nu_{\text{eff}} = n_e e^2 \eta_{\text{eff}} / m_e \sim 2.5 \Omega_{ci} = 0.012 \omega_{pe}$, which is the value obtained by Vlasov code simulations of phase space structures due to current instabilities⁶⁰ and only an order of magnitude smaller than the upper limit of the ideal effective turbulent collision frequency conjectured by Buneman ($0.1 \omega_{pe}$ ⁶¹).

Acknowledgments

We acknowledge the developers of the ACRONYM code (Verein zur Förderung kinetischer Plasmasimulationen e.V.). In particular, we are most grateful to Patrick Kilian for his helpful discussions and valuable comments. We acknowledge funding by the Max-Planck/Princeton Center for Plasma Physics and PRACE (project prj.1602-008) for access to computational resources on the Beskow cluster at PDC/KTH, Sweden.

References

- ¹V. V. Zharkova, K. Arzner, A. O. Benz, P. Browning, C. Dauphin, A. G. Emslie, L. Fletcher, E. P. Kontar, G. Mann, M. Onofri, V. Petrosian, R. Turkmani, N. Vilmer, and L. Vlahos, "Recent Advances in Understanding Particle Acceleration Processes in Solar Flares," *Space Sci. Rev.* **159**, 357–420 (2011), [arXiv:1110.2359](#).
- ²N. Vilmer, "Solar flares and energetic particles," *Philos. Trans. R. Soc. A Math. Phys. Eng. Sci.* **370**, 3241–3268 (2012).
- ³M. Øieroset, R. P. Lin, T. D. Phan, D. E. Larson, and S. D. Bale, "Evidence for Electron Acceleration up to 300 keV in the Magnetic Reconnection Diffusion Region of Earth's Magnetotail," *Phys. Rev. Lett.* **89**, 195001 (2002).
- ⁴J. L. Burch, R. B. Torbert, T. D. Phan, and et. al., "Electron-scale measurements of magnetic reconnection in space," *Science* **352**, aaf2939 (2016).
- ⁵D. L. Turner, J. F. Fennell, J. B. Blake, J. H. Clemmons, B. H. Mauk, I. J. Cohen, A. N. Jaynes, J. V. Craft, F. D. Wilder, D. N. Baker, G. D. Reeves, D. J. Gershman, L. A. Avano, J. C. Dorelli, B. L. Giles, C. J. Pollock, D. Schmid, R. Nakamura, R. J. Strangeway, C. T. Russell, A. V. Artemyev, A. Runov, V. Angelopoulos, H. E. Spence, R. B. Torbert, and J. L. Burch, "Energy limits of electron acceleration in the plasma sheet during substorms: A case study with the Magnetospheric Multiscale (MMS) mission," *Geophys. Res. Lett.* **43**, 7785–7794 (2016).
- ⁶L.-J. Chen, M. Hesse, S. Wang, D. Gershman, R. Ergun, C. Pollock, R. Torbert, N. Bessho, W. Daughton, J. Dorelli, B. Giles, R. Strangeway, C. Russell, Y. Khotyaintsev, J. Burch, T. Moore, B. Lavraud, T. Phan, and L. Avano, "Electron energization and mixing observed by MMS in the vicinity of an electron diffusion region during magnetopause reconnection," *Geophys. Res. Lett.* **43**, 6036–6043 (2016).
- ⁷A. N. Jaynes, D. L. Turner, F. D. Wilder, A. Osmane, D. N. Baker, J. B. Blake, J. F. Fennell, I. J. Cohen, B. H. Mauk, G. D. Reeves, R. E. Ergun, B. L. Giles, D. J. Gershman, R. B. Torbert, and J. L. Burch, "Energetic electron acceleration observed by MMS in the vicinity of an X-line crossing," *Geophys. Res. Lett.* **43**, 7356–7363 (2016).
- ⁸M. Yamada, R. M. Kulsrud, and H. Ji, "Magnetic reconnection," *Rev. Mod. Phys.* **82**, 603–664 (2010).
- ⁹R. A. Treumann and W. Baumjohann, "Spontaneous magnetic reconnection," *Astron. Astrophys. Rev.* **23**, 4 (2015).
- ¹⁰P. Wood and T. Neukirch, "Electron Acceleration in Reconnecting Current Sheets," *Sol. Phys.* **226**, 73–95 (2005).
- ¹¹V. V. Zharkova and M. Gordovskyy, "Energy spectra of particles accelerated in a reconnecting current sheet with the guiding magnetic field," *Mon. Not. R. Astron. Soc.* **356**, 1107–1116 (2005).
- ¹²M. Gordovskyy, P. K. Browning, and G. E. Vekstein, "Particle acceleration in a transient magnetic reconnection event," *Astron. Astrophys.* **519**, A21 (2010).
- ¹³Y. Li and J. Lin, "Acceleration of Electrons and Protons in Reconnecting Current Sheets Including Single or Multiple X-points," *Sol. Phys.* **279**, 91–113 (2012).
- ¹⁴X. Zhou, J. Büchner, M. Bárta, W. Gan, and S. Liu, "Electron Acceleration By Cascading Reconnection In The Solar Corona. I. Magnetic Gradient And Curvature Drift Effects," *Astrophys. J.* **815**, 6 (2015), [arXiv:1504.06486v1](#).
- ¹⁵L. Vlahos, H. Isliker, and F. Lepreti, "Particle Acceleration in an Evolving Network of Unstable Current Sheets," *Astrophys. J.* **608**, 540–553 (2004), [arXiv:0402645 \[astro-ph\]](#).
- ¹⁶R. Turkmani, P. J. Cargill, K. Galsgaard, L. Vlahos, and H. Isliker, "Particle acceleration in stochastic current sheets in stressed coronal active regions," *Astron. Astrophys.* **449**, 749–757 (2006).
- ¹⁷G. Kowal, E. M. de Gouveia Dal Pino, and A. Lazarian, "Particle Acceleration in Turbulence and Weakly Stochastic Reconnection," *Phys. Rev. Lett.* **108**, 241102 (2012), [arXiv:1202.5256](#).
- ¹⁸L. Vlahos, T. Pisokas, H. Isliker, V. V. Tsiolis, and A. Anastasiadis, "Particle Acceleration and Heating by Turbulent Reconnection," *Astrophys. J.* **827**, L3 (2016), [arXiv:arXiv:1604.05234v4](#).
- ¹⁹M. Melzani, R. Walder, D. Folini, C. Winisdoer, and J. M. Favre, "The energetics of relativistic magnetic reconnection : ion-electron repartition and particle distribution hardness," *Astron. Astrophys.* **570**, A112 (2014), [arXiv:1405.2938v1](#).
- ²⁰F. Guo, X. Li, H. Li, W. Daughton, B. Zhang, N. Lloyd-Ronning, Y.-H. Liu, H. Zhang, and W. Deng, "Efficient Production of High-Energy Nonthermal Particles During Magnetic Reconnection in a Magnetically Dominated Ionospheric Electron Plasma," *Astrophys. J.* **818**, L9 (2016).
- ²¹G. R. Werner, D. A. Uzdensky, M. C. Begelman, B. Cerutti, and K. Nalewajko, "Nonthermal particle acceleration in collisionless relativistic electron-proton reconnection," [arXiv preprint \(2016\)](#), [arXiv:1612.04493](#).
- ²²S. R. Titorica, T. Abel, and F. Fiuza, "Non-Thermal Electron Energization from Magnetic Reconnection in Laser-Driven Plasmas," *Phys. Rev. Lett.* **116**, 095003 (2016), [arXiv:1601.05845](#).
- ²³M. Hoshino, T. Mukai, T. Terasawa, and I. Shinohara, "Suprathermal electron acceleration in magnetic reconnection," *J. Geophys. Res. Space Phys.* **106**, 25979–25997 (2001).
- ²⁴P. L. Pritchett, "Relativistic electron production during guide field magnetic reconnection," *J. Geophys. Res.* **111**, A10212 (2006).

- ²⁵W. Wan, G. Lapenta, G. L. Delzanno, and J. Egedal, “Electron acceleration during guide field magnetic reconnection,” *Phys. Plasmas* **15**, 032903 (2008).
- ²⁶J. Egedal, W. Daughton, and A. Le, “Large-scale electron acceleration by parallel electric fields during magnetic reconnection,” *Nat. Phys.* **8**, 321–324 (2012).
- ²⁷J. F. Drake, M. Swisdak, H. Che, and M. A. Shay, “Electron acceleration from contracting magnetic islands during reconnection,” *Nature* **443**, 553–556 (2006).
- ²⁸J. F. Drake, M. Opher, M. Swisdak, and J. N. Chamoun, “A magnetic reconnection mechanism for the generation of anomalous cosmic rays,” *Astrophys. J.* **709**, 963–974 (2010).
- ²⁹M. Hoshino, “Stochastic Particle Acceleration in Multiple Magnetic Islands during Reconnection,” *Phys. Rev. Lett.* **108**, 135003 (2012), [arXiv:1201.0837](https://arxiv.org/abs/1201.0837).
- ³⁰J. F. Drake, M. Swisdak, and R. Fermo, “the Power-Law Spectra of Energetic Particles During Multi-Island Magnetic Reconnection,” *Astrophys. J.* **763**, L5 (2013).
- ³¹J. T. Dahlin, J. F. Drake, and M. Swisdak, “The Mechanisms of Electron Heating and Acceleration during Magnetic Reconnection,” *Phys. Plasmas* **21**, 092304 (2014), [arXiv:1406.0831](https://arxiv.org/abs/1406.0831).
- ³²X. Li, F. Guo, H. Li, and G. Li, “Nonthermally Dominated Electron Acceleration During Magnetic Reconnection in a Low-beta Plasma,” *Astrophys. J.* **811**, L24 (2015), [arXiv:1505.02166v1](https://arxiv.org/abs/1505.02166v1).
- ³³J. T. Dahlin, J. F. Drake, and M. Swisdak, “Parallel electric fields are inefficient drivers of energetic electrons in magnetic reconnection,” *Phys. Plasmas* **23**, 120704 (2016).
- ³⁴G. P. Zank, J. A. le Roux, G. M. Webb, A. Dosch, and O. Khabarova, “Particle Acceleration Via Reconnection Processes in the Supersonic Solar Wind,” *Astrophys. J.* **797**, 28 (2014).
- ³⁵O. Khabarova, G. P. Zank, G. Li, J. A. le Roux, G. M. Webb, A. Dosch, and O. E. Malandraki, “Small-scale magnetic islands in the solar wind and their role in particle acceleration. I. Dynamics of magnetic islands near the heliospheric current sheet,” *Astrophys. J.* **808**, 181 (2015).
- ³⁶J. T. Dahlin, J. F. Drake, and M. Swisdak, “Electron acceleration in three-dimensional magnetic reconnection with a guide field,” *Phys. Plasmas* **22**, 100704 (2015), [arXiv:1503.02218](https://arxiv.org/abs/1503.02218).
- ³⁷P. A. Muñoz, D. Told, P. Kilian, J. Büchner, and F. Jenko, “Gyrokinetic and kinetic particle-in-cell simulations of guide-field reconnection. I. Macroscopic effects of the electron flows,” *Phys. Plasmas* **22**, 082110 (2015), [arXiv:1504.01351](https://arxiv.org/abs/1504.01351).
- ³⁸P. Kilian, T. Burkart, and F. Spanier, “The Influence of the Mass Ratio on Particle Acceleration by the Filamentation Instability,” in *High Performance Computing in Science and Engineering '11*, edited by W. E. Nagel, D. B. Kröner, and M. M. Resch (Springer Berlin Heidelberg, Berlin, Heidelberg, 2012) pp. 5–13.
- ³⁹J. May, J. Tonge, I. Ellis, W. B. Mori, F. Fiuza, R. A. Fonseca, L. O. Silva, and C. Ren, “Enhanced stopping of macro-particles in particle-in-cell simulations,” *Phys. Plasmas* **21**, 052703 (2014), [arXiv:1401.1198](https://arxiv.org/abs/1401.1198).
- ⁴⁰J. F. Drake, “Formation of Electron Holes and Particle Energization During Magnetic Reconnection,” *Science* **299**, 873–877 (2003).
- ⁴¹P. L. Pritchett and F. V. Coroniti, “Three-dimensional collisionless magnetic reconnection in the presence of a guide field,” *J. Geophys. Res.* **109**, A01220 (2004).
- ⁴²H. Che, J. F. Drake, and M. Swisdak, “A current filamentation mechanism for breaking magnetic field lines during reconnection,” *Nature* **474**, 184–187 (2011).
- ⁴³D. E. Wendel, D. K. Olson, M. Hesse, N. Aunai, M. Kuznetsova, H. Karimabadi, W. Daughton, and M. L. Adrian, “The relation between reconnected flux, the parallel electric field, and the reconnection rate in a three-dimensional kinetic simulation of magnetic reconnection,” *Phys. Plasmas* **20**, 122105 (2013).
- ⁴⁴P. L. Pritchett, F. S. Mozer, and M. Wilber, “Intense perpendicular electric fields associated with three-dimensional magnetic reconnection at the subsolar magnetopause,” *J. Geophys. Res.* **117**, A06212 (2012).
- ⁴⁵V. Roytershteyn, W. Daughton, H. Karimabadi, and F. S. Mozer, “Influence of the Lower-Hybrid Drift Instability on Magnetic Reconnection in Asymmetric Configurations,” *Phys. Rev. Lett.* **108**, 185001 (2012).
- ⁴⁶S. Markidis, G. Lapenta, A. Divin, M. Goldman, D. Newman, and L. Andersson, “Three dimensional density cavities in guide field collisionless magnetic reconnection,” *Phys. Plasmas* **19**, 032119 (2012).
- ⁴⁷Y. V. Khotyaintsev, A. Vaivads, M. André, M. Fujimoto, A. Retinò, and C. J. Owen, “Observations of Slow Electron Holes at a Magnetic Reconnection Site,” *Phys. Rev. Lett.* **105**, 165002 (2010).
- ⁴⁸F. S. Mozer and P. L. Pritchett, “Spatial, temporal, and amplitude characteristics of parallel electric fields associated with subsolar magnetic field reconnection,” *J. Geophys. Res. Space Phys.* **115**, A04220 (2010).
- ⁴⁹R. E. Ergun, J. C. Holmes, K. A. Goodrich, F. D. Wilder, J. E. Stawarz, S. Eriksson, D. L. Newman, S. J. Schwartz, M. V. Goldman, A. P. Sturmer, D. M. Malaspina, M. E. Usanova, R. B. Torbert, M. Argall, P.-A. Lindqvist, Y. Khotyaintsev, J. L. Burch, R. J. Strangeway, C. T. Russell, C. J. Pollock, B. L. Giles, J. J. C. Dorelli, L. Avanov, M. Hesse, L. J. Chen, B. Lavraud, O. Le Contel, A. Retino, T. D. Phan, J. P. Eastwood, M. Oieroset, J. Drake, M. A. Shay, P. A. Cassak, R. Nakamura, M. Zhou, M. Ashour-Abdalla, and M. André, “Magnetospheric Multiscale observations of large-amplitude, parallel, electrostatic waves associated with magnetic reconnection at the magnetopause,” *Geophys. Res. Lett.* **43**, 5626–5634 (2016).
- ⁵⁰L. S. Shepherd and P. A. Cassak, “Guide field dependence of 3-D X-line spreading during collisionless magnetic reconnection,” *J. Geophys. Res. Space Phys.* **117**, A10101 (2012).
- ⁵¹S. Dorfman, H. Ji, M. Yamada, J. Yoo, E. Lawrence, C. Myers, and T. D. Tharp, “Experimental observation of 3-D, impulsive reconnection events in a laboratory plasma,” *Phys. Plasmas* **21**, 012109 (2014).
- ⁵²J. D. Huba and L. I. Rudakov, “Three-dimensional Hall magnetic reconnection,” *Phys. Plasmas* **9**, 4435 (2002).
- ⁵³N. Jain, J. Büchner, S. Dorfman, H. Ji, and A. Surjalal Sharma, “Current disruption and its spreading in collisionless magnetic reconnection,” *Phys. Plasmas* **20**, 112101 (2013).
- ⁵⁴J. Büchner and J. Kuska, “Sausage mode instability of thin current sheets as a cause of magnetospheric substorms,” *Ann. Geophys.* **17**, 604–612 (1999).
- ⁵⁵G. Lapenta, D. Krauss-Varban, H. Karimabadi, J. D. Huba, L. I. Rudakov, and P. Ricci, “Kinetic simulations of x-line expansion in 3D reconnection,” *Geophys. Res. Lett.* **33**, L10102 (2006).
- ⁵⁶T. G. Northrop, “Adiabatic charged-particle motion,” *Rev. Geophys.* **1**, 283 (1963).
- ⁵⁷G. D. Holman, L. Sui, R. A. Schwartz, and A. G. Emslie, “Electron Bremsstrahlung Hard X-Ray Spectra, Electron Distributions, and Energetics in the 2002 July 23 Solar Flare,” *Astrophys. J.* **595**, L97–L101 (2003).
- ⁵⁸E. P. Kontar, N. H. Bian, A. G. Emslie, and N. Vilmer, “Turbulent Pitch-Angle Scattering and Diffusive Transport of Hard X-Ray-Producing Electrons in Flaring Coronal Loops,” *Astrophys. J.* **780**, 176 (2014).
- ⁵⁹N. Bessho and A. Bhattacharjee, “Fast Magnetic Reconnection and Particle Acceleration in Relativistic Low-density Electron-Positron Plasmas without Guide Field,” *Astrophys. J.* **750**, 129 (2012).
- ⁶⁰J. Büchner and N. Elkina, “Anomalous resistivity of current-driven isothermal plasmas due to phase space structuring,” *Phys. Plasmas* **13**, 082304 (2006).
- ⁶¹O. Buneman, “Instability, Turbulence, and Conductivity in Current-Carrying Plasma,” *Phys. Rev. Lett.* **1**, 8–9 (1958).